analytical chemistry

pubs.acs.org/ac Article

Enzymes-Encapsulated Defective Metal–Organic Framework Hydrogel Coupling with a Smartphone for a Portable Glucose Biosensor

Ningyi Zhong, Rui Gao, Yujian Shen, Xiaoxue Kou, Jiayi Wu, Siming Huang,* Guosheng Chen,* and Gangfeng Ouyang

Cite This: *Anal. Chem.* 2022, 94, 14385−14393 Read Online

ACCESS | Metrics & More | Article Recommendations | Supporting Information

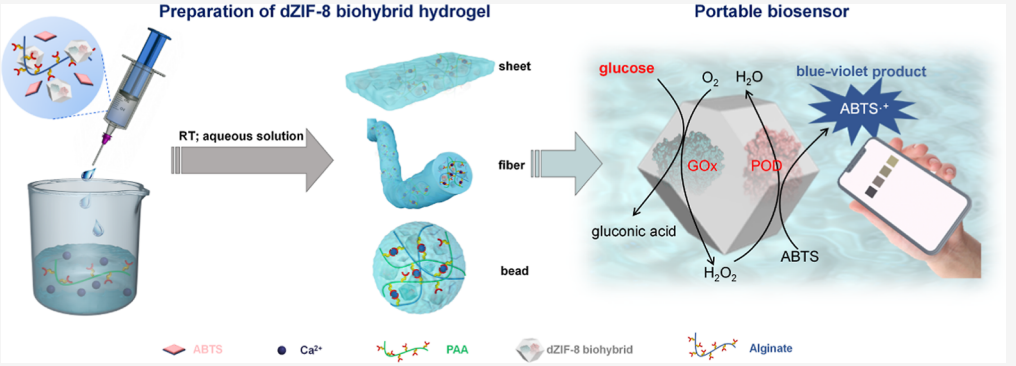

ABSTRACT: Enzymes featuring high catalytic efficiency and selectivity have been widely used as the sensing element in analytical chemistry. However, the structural fragility and poor machinability of an enzyme significantly limit its practicability in biosensors. Herein, we develop a robust and sensitive hybrid biosensor by means of co-encapsulating enzymes into a defective metal−organic framework (MOF), followed by a double-crosslinked alginate gelatinization. The defective MOF encapsulation can enhance the stability of enzymes, yet well preserve their biocatalytic function, while the alginate gelatinization allows the MOF biohybrid high stretchability and mechanical strength, which facilitates the integration of a bead-, fiber-, and sheet-like portable biosensor. In this work, the enzymes consisting of glucose oxidase and peroxidase are co-encapsulated into this MOF hydrogel, and it can efficiently convert glucose into a blue-violet product through the biocatalytic cascade of encapsulated enzymes, enabling the colorimetric biosensing of glucose on a miniaturized MOF hydrogel when coupling with a smartphone. Interestingly, this MOF biohybrid hydrogel outputs a stronger sensing signal than the free biohybrid powders, attributed to the catalytic product-accumulated effect of the highly hydrophilic microenvironment of the hydrogel. As a result, this portable biosensor can sensitively and selectively sense glucose with a linear range from 0.05 to 4 mM. Importantly, both the hydrophilic hydrogel and MOF "armor" endow enzymes with high durability, and its sensing activity was well-maintained even after placing the biosensor at room temperature for 30 d. We believe that this MOF biohybrid hydrogel has huge potential for the engineering of next-generation portable biosensors.

Portable biosensors are miniaturized and function-integrated sensors that afford real-time detection results at the point of care, which well circumvent the shortcomings of laboratory-based screening techniques, such as delayed feedback and high cost.[1,2] They are highly desirable in personalized medicine and continuous health monitoring of globally transmitted life-threatening epidemics.[3−5] With regard to the desirable biosensors, conceiving the portable sensing element featuring high sensitivity and selectivity is of significant importance. Biocascade, a continuous catalytic reaction driven by enzymes, is an essential metabolic pathway in living cells.[6−8] Since it permits efficient signal transmission and feedback in complex cellular networks through mild enzymatic catalysis, this natural cascade has offered new opportunities for implementing various sensing routes that have previously not been achieved by artificial units.[9,10] Unfortunately, enzymes are environment-susceptive biopolymers, and the spatial immobilization of fragile enzymes utilizing solid supports is necessary to preserve enzymatic function in an extracellular environment.[11,12]

Received: July 20, 2022
Accepted: September 29, 2022
Published: October 7, 2022

https://doi.org/10.1021/acs.analchem.2c03138
Anal. Chem. 2022, 94, 14385−14393

Scheme 1. Schematic Representation of the Preparation of dZIF-8 BH through Double-Crosslinked Alginate Gelatinization and the Colorimetric Sensing Mechanism Based on the Biocatalytic Cascade of dZIFs BH

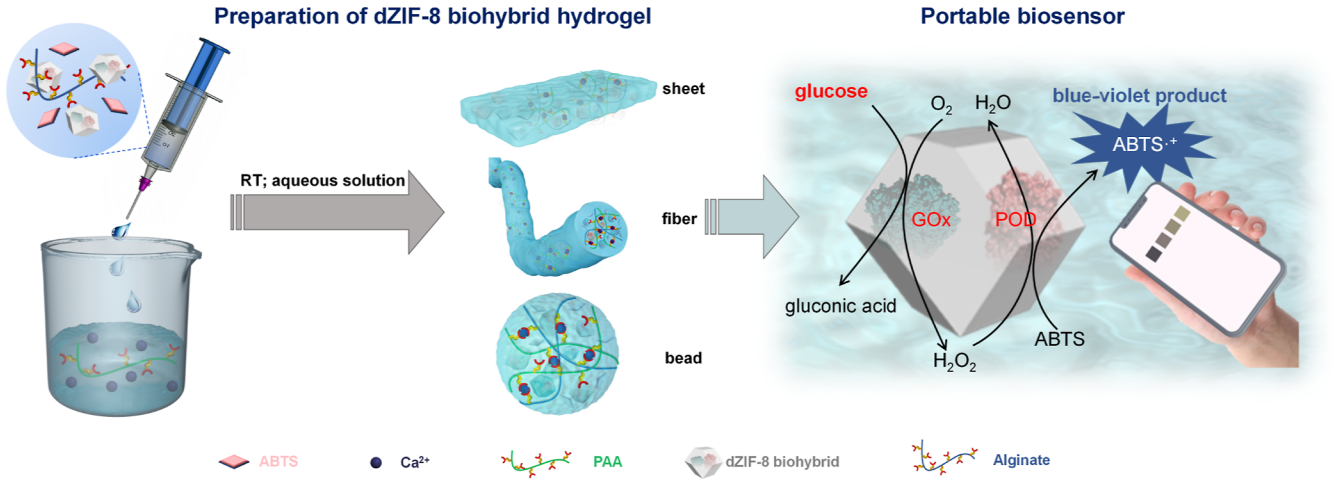

Metal−organic frameworks (MOFs), a class of reticular hybrid materials linked by organic ligands and metal nodes, have been considered as the ideal supports for enzyme immobilization and showcase distinct merits.[13,14] On one hand, the ultrahigh specific surface areas of MOFs provide sufficient spaces for loading or spatially organizing the cargos within their cavities. On the other hand, the customizable topology not only tightly confines the enzymes but also allows the selective entrance of substrates as well as the timely transport of subsequent intermediates and products, facilitating the biocascade process in a confined MOF environment.[15] To this point, zeolite imidazole frameworks (ZIFs), including ZIF-8, ZIF-90, MAF-7, and so forth, are the favorable MOF matrices for enzyme immobilization due to their biocompatible synthesis conditions.[16−20] A pioneering work by Liang, Falcaro, and co-workers has found that ZIF-8 could in situ crystallize around a given enzyme, analogous to the natural biomineralization.[21] Utilizing this method, single or multiple enzymes are readily encapsulated into ZIFs, and the encapsulated enzymes display improved stability yet maintain desirable bioactivity.[22−29] However, these ZIFs biohybrids are microcrystalline powders and hence are difficult to be mechanically processed and shaped in a controllable manner. This significantly limits the MOF biohybrid acting as the core element in large-scale industrial applications, such as portable biosensors.

Alginate is a class of natural polysaccharides that enables the crosslink with divalent cations (such as Ca^{2+}, Zn^{2+}, and Co^{2+}) into a hydrogel in an aqueous solution.[30−32] Inspired by the green and mild crosslinking pathway as well as the water-stable structure of the alginate hydrogel, herein, we reported a morphology-adjustable defective ZIF biohybrid hydrogel (dZIF-8 BH) through a double-crosslinked alginate gelatinization and subsequently explored its biocatalytic cascade performance for developing a portable biosensor (Scheme 1). To strengthen the mechanical property, an additional crosslinker, poly(acrylic acid) (PAA), was introduced. Such double-crosslinked "bio-glue" readily shaped the dZIF biohybrid and the signal molecule 2,2′-azinobis(2-ethylbenzthiazoline-6-sulfonate) (ABTS) into monolithic bead, fiber, or film structures. The formed dZIFs BH possessed high mechanical strength and stretchability and could accumulate the biocascade product ($ABTS^{\bullet+}$), apparently displaying a stronger catalytic signal in function of the same substrate concentration than that of the free enzyme@ZIFs powders. Importantly, the highly hydrophilic environment, created by the hydrogel layer, further improved the stability of the encapsulated enzymes. It permitted the fabricated biosensor with well-preserved bioactivity after placing at room temperature for 30 d. We believe that this dZIF-8 BH with high processibility and sensing performance has huge potential for the engineering of next-generation portable biosensors.

METHODS

Synthesis of Defective Enzymes−ZIF-8 Biohybrid. The defective ZIF-8 (dZIF-8) biohybrid was synthesized through a biomineralization method.[21] In this process, 10 mg of enzymes consisting of 5 mg of peroxidase (POD) and 5 mg of glucose oxidase (GOx) was dispersed into 5 mL of 2-methylimidazole (HmIM) solution (160 mM) through ultrasonic treatment, followed by adding 5 mL of zinc acetate solution (40 mM). Then, the mixed system was aged for 4 h at room temperature. Finally, the precipitate was collected by centrifugation and washed by deionized water three times.

Fluorescence Labeling of Enzymes. The dyes labeling of enzymes was referred by our previous report.[33,34] For rhodamine B (RhB)-labeled POD, 20 mg of POD was dispersed into 10 mL of carbonate buffer (pH = 8.0, 0.5 M), followed by introducing 1 mg of RhB isothiocyanate. The mixture was then stirred for 4 h in dark conditions.

For fluorescein isothiocyanate (FITC)-labeled GOx, 20 mg of GOx was dispersed into 10 mL of carbonate buffer (pH = 9.0, 0.5 M), followed by introducing 1 mg of FITC. The mixture was then stirred for 4 h in dark conditions.

Finally, RhB-labeled POD and FITC-labeled GOx were, respectively, obtained through an ultrafiltration method using a centrifugal filter device (molecular weight cutoff MWCO = 8 kDa) performed three times to remove the excess reaction reagents and salts. The products were dried by lyophilization.

Synthesis of FITC-Labeled GOx@dZIF-8. 10 mg of FITC-labeled GOx was dispersed into 5 mL of HmIM solution (160 mM) through ultrasonic treatment, followed by adding 5 mL of zinc acetate solution (40 mM). Then, the mixed solution was aged for 4 h at room temperature. Finally, the

https://doi.org/10.1021/acs.analchem.2c03138
Anal. Chem. 2022, 94, 14385−14393

precipitate was collected by centrifugation and washed with deionized water three times.

Synthesis of RhB-Labeled POD@dZIF-8. 5 mg of RhB-labeled POD and 5 mg of bovine serum albumin (BSA) were dispersed into 5 mL of HmIM solution (160 mM) through ultrasonic treatment, followed by adding 5 mL of zinc acetate solution (40 mM). Then, the mixed solution was aged for 4 h at room temperature. Finally, the precipitate was collected by centrifugation and washed with deionized water three times.

Quantification of the Loading Efficiency of Each Enzyme in dZIF-8. The loadings of POD and GOx in dZIF-8 biohybrids were evaluated by using RhB-labeled POD and FITC-labeled GOx instead of raw POD and GOx, respectively, in the synthesis procedure of the dZIF-8 biohybrid. The enzyme loadings were measured by examining the corresponding fluorescence decrease in the supernatant before and after encapsulation via fluorescence spectra. The FITC-labeled GOx and RhB-labeled POD were quantified at 518 nm (488 nm excitation) and 582 nm (560 nm excitation), respectively.

Synthesis of the dZIF-8 Biohybrid Hydrogel. 40 mg of the as-synthesized dZIF-8 biohybrid powders was dispersed uniformly in 1 mL of 5 mM ABTS solution by ultrasonication. After the dispersion, the suspension was magnetically stirred, and 20 mg of sodium alginate was then added to form a mixed solution **A**.

$CaCl_2$ (60 M) was dissolved into 0.05 M PAA solution, and a mixed solution **B** was formed.

For the bead-like and fiber-like dZIF-8 BH, solution **A** was loaded into a 1 mL commercial syringe and then carefully dropped or directly injected into solution **B**. A bead-like or fiber-like dZIF-8 BH was generated upon the mixing of solution **A** and solution **B**.

For the sheet-like dZIF-8 BH, solution **A** was evenly coated onto a glass plate using a coating machine (Figure S14), and the thickness was set to 0.4 mm; the above-mentioned glass plate was then horizontally immersed into solution **B** and polymerized for 10 min to generate a sheet-like dZIF-8 BH.

RGB Color Recognition Using a Smartphone Application. In order to realize the portable biosensing, the catalytic RGB color signal was directly photographed and analyzed using a smartphone application, named Color Picker (Figure S15a). Notably, the snapshot process was carried out in a cabinet under light-emitting diode (LED) light (Figure S15b) for ensuring the stability of the environmental light condition.

The flow chart of the color analysis using the Color Picker App includes snapshot and color scan, as shown in Figure S15. The as-prepared dZIF-8 BH sheet (0.5 cm × 0.5 cm) was washed with deionized water to remove the unwanted impurities and then placed into the center of the cabinet while the LED light was turned on. The image of this raw dZIF-8 BH sheet was recorded using the smartphone camera, which was named as image **A**. Subsequently, 5 μL of the glucose sample was added onto the center of the dZIF-8 BH sheet using a pipette, and after the biocatalytic cascade reaction was allowed to proceed for a certain time at room temperature, the image of the sheet was recorded again, which was named as image **B**.

After the snapshot, images **A** and **B** were directly loaded from the smartphone album, and the red−green−blue (RGB) values of each pixel from the touchscreen area were directly outputted using the color scan function of the App (Figure S15c). Notably, for each image, the R, G, or B value was the average one from nine different touchscreen areas. Herein, the ΔR value, that is, the difference value of the R values of images **B** and **A**, was chosen as the color parameter for the quantification, and an excellent linear relationship was observed between ΔR and glucose ranging from 0.05 to 0.25 mM or from 0.25 to 4 mM.

Anti-interference Test. For examining the anti-interference ability of the dZIF-8 BH sheet, 14 kinds of routine biomolecules, including fructose, xylose, rhamnose, sucrose, lactose, galactose, maltose, glycine, BSA, urea, histidine, arginine, glutamate, and alanine, were selected as the interferents. Briefly, 5 μL of a 10-fold high concentration of the interferent (10 mM) was added onto the center of the dZIF-8 BH sheet, respectively. After the incubation for 15 min, the ΔR value of each interferent was obtained using the above-mentioned RGB-App. Herein, the ΔR value of 5 μL of 1 mM glucose was set as the benchmark for evaluating the anti-interference ability.

Cross-Reactivity Measurement. For evaluating the cross-reactivity, 5 μL of a glucose solution (1 mM) consisting of 10 mM different interferents was added onto the center of the dZIF-8 BH sheet, respectively. After the incubation for 15 min, the ΔR value of each assay was obtained based on the above-mentioned RGB-App. Herein, the ΔR value of 5 μL of 1 mM glucose was set as the benchmark for evaluating the cross-reactivity.

Storage Stability of the dZIF-8 BH Sheet Biosensor. A series of dZIF-8 BH sheets with a 0.5 cm × 0.5 cm dimension were stored in a closed plastic tube placed at 25 °C. After storing for a time interval, three sheets were randomly taken out, and 5 μL of glucose (1 mM) was added onto the center of each sheet. After 15 min incubation, the ΔR value in average (denoted as $\Delta R_{\text{after storage}}$, $n = 3$) was obtained based on the above-mentioned RGB-App. The retained sensing activity, which was calculated based on eq 1, was used for the evaluation of the stability of the biosensor

$$\text{the retained sensing activity (\%)} = \Delta R_{\text{after storage}}/\Delta R_{\text{original}} \times 100\% \quad (1)$$

wherein the $\Delta R_{\text{original}}$ was defined as the ΔR value in average at day 0.

Enzyme Leaching Experiment. The dZIF-8 BH beads and the enzymes-embedded hydrogel beads (each enzyme loading was kept the same in these two hydrogel beads) were dispersed in 5 mL of deionized water and shook for 12 h at room temperature. The supernatant was collected, and the leached enzymes were measured by a standard Bradford assay.[35]

RESULTS AND DISCUSSION

Structure and Cascade Activity of Defective Enzymes@ZIF-8. As a proof of concept, a typical biocascade consisting of GOx and POD was chosen as the sensing unit.[9] This biocascade could be used for visually sensing glucose, a biomarker of diabetes, when combining the hydrogen donor molecule ABTS (Scheme 1). The previous research by our group has identified that the biomineralization of ZIF-8 under a low ratio of HmIM (an organic linker of ZIF-8) to the metal (Zn^{2+}) precursor was facile to form a defective ZIF-8 (dZIF-8)-encapsulated enzyme nanostructure, and the defective cavity could promote the mass transfer that improved the biocatalytic activity.[26] Given this discovery, the GOx and POD

https://doi.org/10.1021/acs.analchem.2c03138
Anal. Chem. 2022, 94, 14385−14393

were co-encapsulated into dZIF-8 under a low ratio of HmIM to the Zn^{2+} precursor. The formed dZIF-8 biohybrids inherited the standard Bragg diffraction pattern of SOD-type ZIF-8 (Figure S1), and the crystalline domains were also confirmed by cryo-EM, wherein the (211) lattice plane was clearly identified in some dZIF-8 domains (Figure S2). In addition, the successful encapsulation of enzymes into the dZIF-8 shell was evidenced by several characterizations, including Fourier transform infrared (FT-IR) spectroscopy, thermogravimetric analysis (TGA), and the N_2 adsorption isothermal analysis (details can be seen in Figures S3−S5). For exploring the spatial distribution of the enzymes, GOx and POD were, respectively, labeled by FITC (a green fluorescence dye) and RhB (a red fluorescence dye) before the encapsulation. The loadings of each enzyme, calculated by the fluorescence intensity change before and after encapsulation in the supernatant (Figure S6), were measured to be 19.0% (w/w) and 12.1% (w/w) for GOx and POD, respectively. The closer examination by confocal laser scanning microscopy (CLSM) images clearly observed the uniform distribution of FITC-labeled GOx and RhB-labeled POD within a dZIF-8 crystal (Figure S7).

Notably, ZIF-8 has a ca. 12 Å honeycomb-like cavity connected by HmIM and Zn clusters, and the pore window was as small as 3.4 Å viewing from the [110] projection.[36] Therefore, introducing the defective structure is essential for enhancing the accessibility of the enzymes, which enables the biosensor with high sensitivity. The insight into the defective domains of the synthesized dZIF-8 biohybrid was further examined by integrated differential phase contrast scanning transmission electron microscopy (iDPC-STEM), a new low-electronic dosage transmission electron microscopy (TEM) technique with high resolution and signal-to-noise ratio.[37,38] We directly identified the abundant defective and crystalline domains within the crystal from the [110] projection (Figure 1a). Such a multiphase structure ensured the free entrance of the glucose into the confined enzymes, after which the biocascade was activated. As a result, the sensing activity of this dZIF-8 biohybrid, in terms of the amount of the blue-violet product ($ABTS^{\bullet+}$) after 5 min of the biocascade reaction, was comparable to that of the free GOx−POD counterpart in the identical enzyme dosages (Figure 1b), even though the sensing rate was slightly inhibited by the dZIF-8 shell after encapsulation.

To clarify the positive role of co-encapsulating enzymes within a dZIF crystal for cascade catalysis, we also separately encapsulated GOx (labeled by FITC) and POD (labeled by RhB) into dZIF-8 using the similar encapsulation method, and the dZIF-8 biohybrids were denoted as GOx@dZIF-8 and POD@dZIF-8, respectively. The powder X-ray diffraction (PXRD) analysis showed that the synthesized GOx@dZIF-8 and POD@dZIF-8 were highly crystalline (Figure S8a), and the CLSM images demonstrated that the GOx or POD were uniformly distributed within dZIF-8 (Figure S8b). The GOx or POD loadings in dZIF-8 were measured by examining the fluorescence decrease in the supernatant before and after encapsulation via fluorescence spectroscopy, and a 31.4% GOx loading in GOx@dZIF-8 and a 13.5% POD loading in POD@dZIF-8 were obtained. The insight into the catalytic curve showed that when GOx and POD were encapsulated into separated dZIF-8 crystals, the cascade activity was decreased compared with that of dZIF-8 in which GOx and POD were co-encapsulated. The different cascade activities might be

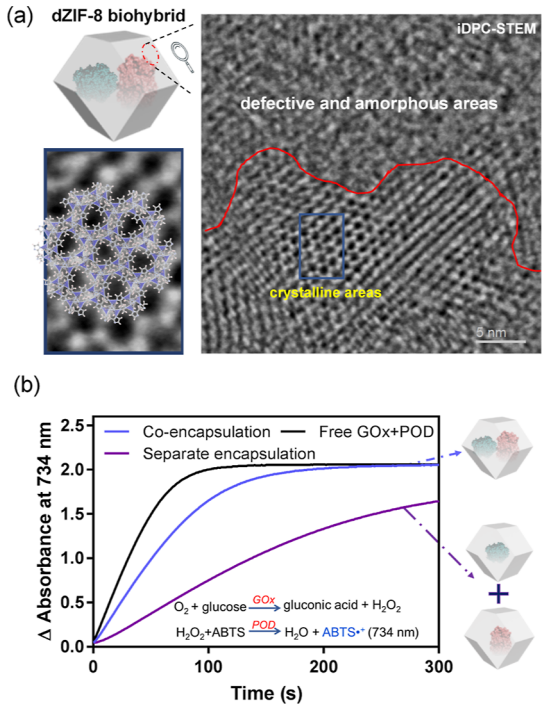

Figure 1. (a) iDPC-STEM revealed the defective and crystalline domains within a dZIF-8 biohybrid powder from the [110] projection. (b) Cascade activity of physically mixed GOx and POD (free GOx + POD), co-encapsulation of GOx and POD within ZIF-8, and separate encapsulation of GOX and POD within ZIF-8, respectively. In order to control the enzyme dosage in both groups, GOx and POD were labeled by FITC and RhB, respectively, and the dosage of each enzyme was kept the same in both groups, POD: 40 μg/mL and GOx: 60 μg/mL. The distinct UV−vis absorbance intensity at 734 nm was used to quantify the cascade product $ABTS^{\bullet+}$.

attributed to the proximity effect.[7] When GOx and POD were confined in one crystal, the diffusion path of the intermedium was significantly shortened, thus promoting the cascade biocatalysis.[22]

Preparation of the Morphology-Adjustable Defective Enzymes@ZIF-8 Hydrogel. Next, dZIF-8 BH was fabricated by the double-crosslinked gelatinization. Briefly, the as-synthesized dZIF-8 biohybrids and ABTS were dispersed into the alginate solution (termed as solution **A**), and the gelatinization was instantaneously activated by introducing solution **A** into solution **B** consisting of Ca^{2+} and PAA (Scheme 1). Utilizing this mild gelatinization strategy, the dZIF-8 biohybrid powders were shapable, while avoiding the risk of denaturation of enzymes. Taking the bead-like dZIF-8 BH as an example, the solution **A** was slowly dropped into solution **B** via a 1 mL commercial injection syringe. A uniform bead with a ca. 1.76 mm diameter was formed once solution **A** was dropped into solution **B** (Figures 2a and S9a). To confirm that dZIF-8 BH was indeed crosslinked to Ca^{2+}, alginate, and PAA, FT-IR spectroscopy was carried out. All FT-IR absorption bands assigned to alginate were clearly recorded in the hydrogel (Figure S10). Specifically, the asymmetric C=O stretching vibration at 1708 cm^{-1}, associated with the free −COOH group of PAA, emerged in the hydrogel. Meanwhile, the O−H stretching vibration at ca. 3436 cm^{-1} was also enhanced compared to that of alginate, attributed to the additional carbonyl −OH groups of PAA.[32] These gave the first evidence of the existence of PAA. The further insights by

https://doi.org/10.1021/acs.analchem.2c03138
Anal. Chem. 2022, 94, 14385−14393

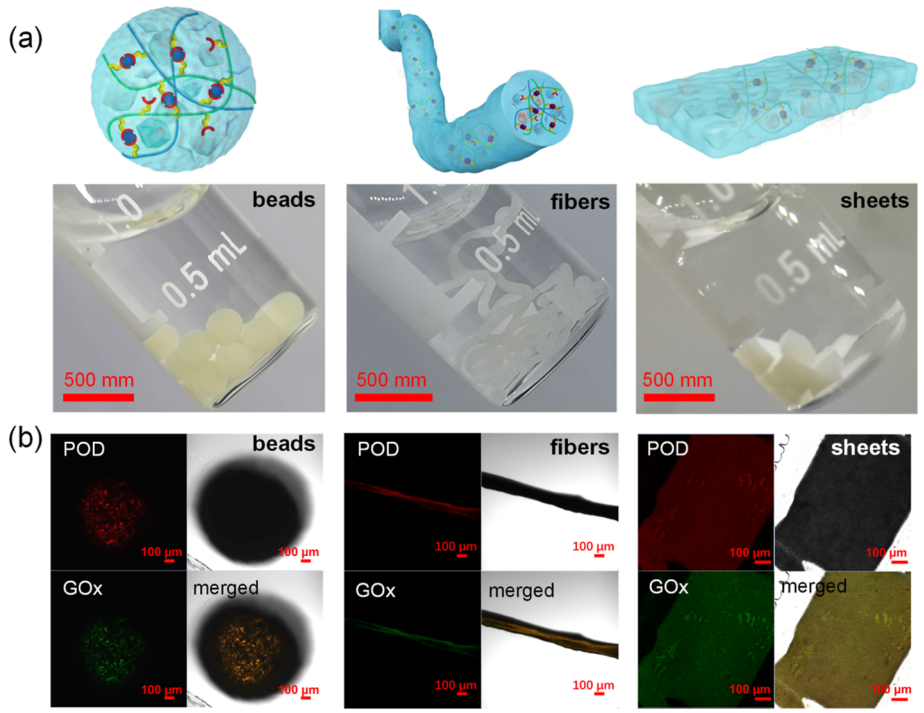

Figure 2. (a) Schematic presentation and digital photographs of the as-prepared dZIF-8 BH with controllable morphologies. (b) CLSM images, in which the POD was labeled by RhB, while GOx was labeled by FITC.

Raman spectra revealed that the ν(C═O) stretching vibration of free carboxyl groups of PAA (at 1692 cm^{-1}) was almost disappeared after the gelatinization, suggesting that the carboxyl of PAA was coordinated with Ca^{2+} ions[39] (Figure S11). In addition, the incorporation of dZIF-8 biohybrids was supported by the scanning electron microscopy (SEM) imaging (Figure S12) and PXRD test (Figure S13), and the calculated loading efficiency was as high as 66.67% in average.

The CLSM imaging revealed that the GOx (labeled by FITC) and POD (labeled by RhB), co-encapsulated within dZIF-8, were evenly distributed in a bead (Figure 2b). Importantly, this gelatinization strategy was also able to shape dZIF-8 BH into other morphologies, such as a fiber and a sheet (Figure 2a). For the fiber, the injection syringe consisting of solution **A** was directly immersed into solution **B**, and then, the solution **B** was continuously infused with solution **A** (Figure S9b). However, for the sheet, the gelatinization process was assisted by a filming coating machine (details can be seen in the Supporting Information, Figures S9c and S14). The dZIF-8 biohybrid powders were uniformly dispersed into both the fiber and sheet, as evidenced by the CLSM imaging (Figure 2b).

Improvement on the Colorimetric Sensing Ability. The sensing performance of the prepared dZIF-8 BH was then evaluated by the time-dependent change of the apparent color under the action of glucose. In the biocatalytic cascade, glucose could be converted into gluconic acid and H_2O_2 by the aerobic catalysis of GOx, while the generated H_2O_2 oxidized the colorless ABTS into the blue-violet $ABTS^{\bullet+}$ by the POD catalyst (Figure 3a). To achieve the goal of constructing a portable biosensor, the RGB color signal of the produced $ABTS^{\bullet+}$ was directly captured using a smart phone camera and subsequently analyzed using a commercial Color Picker Application (details can be seen in the Supporting Information, Figure S15). Interestingly, the kinetic measurements indicated that the sensing capacity of dZIF-8 BH outperformed that of the dZIF-8 biohybrid powders under the same enzyme dosage and same glucose concentration, in which dZIF-8 BH changed from faint yellow into green in the first 10 min and then changed into blue-violet at 15 min (Figure 3b–d). Such a time-dependent color variation was distinguishable by the naked eyes. The enlarged picture showed that the entirety of the dZIF-8 BH turned blue-violet after 15 min (Figure 3b–d), attributed to the highly hydrophilic hydrogel that favored the accumulation of the hydrophilic biocatalytic product, $ABTS^{\bullet+}$. Meanwhile, compared with dZIF-8 BH, the surrounding solution phase displayed a limited color change (Figure S16), further supporting the catalytic product-accumulated effect of the hydrogel. These results suggested that our dZIF-8 BH outputted a more sensitive color signal than free dZIF-8 biohybrid powders in the function of glucose.

Sensitive and Long-Life Portable Biosensor. Given the desirable sensing performance of dZIF-8 BH, we then explored the possibility of constructing a portable biosensor based on this dZIF-8 BH coupled with the all-pervading smartphone. As a proof of concept, the miniaturized and portable dZIF-8 BH sheet with a 0.5 cm × 0.5 cm dimension was used as the integrated biosensor, and 5 μL of the glucose sample was directly dropped into the center of the dZIF-8 BH sheet (Figure 4a). After incubation for 15 min, the ΔR value of the color was directly analyzed on a smartphone (Figure S15). As shown in Figure 4a, the apparent color of the sheet biosensor changed from faint yellow to green as the glucose was increased from 0.05 to 0.25 mM and then gradually turned blue-violet upon a further increase of the glucose from 0.25 to 4 mM. Importantly, the changed color was homogeneous throughout the sheet biosensor owing to the high hydrophilicity of the hydrogel (Figure S17), and such a uniform color was crucial for the accurate readout using a smartphone application. As a result, the ΔR value of the color change of the

https://doi.org/10.1021/acs.analchem.2c03138
Anal. Chem. 2022, 94, 14385−14393

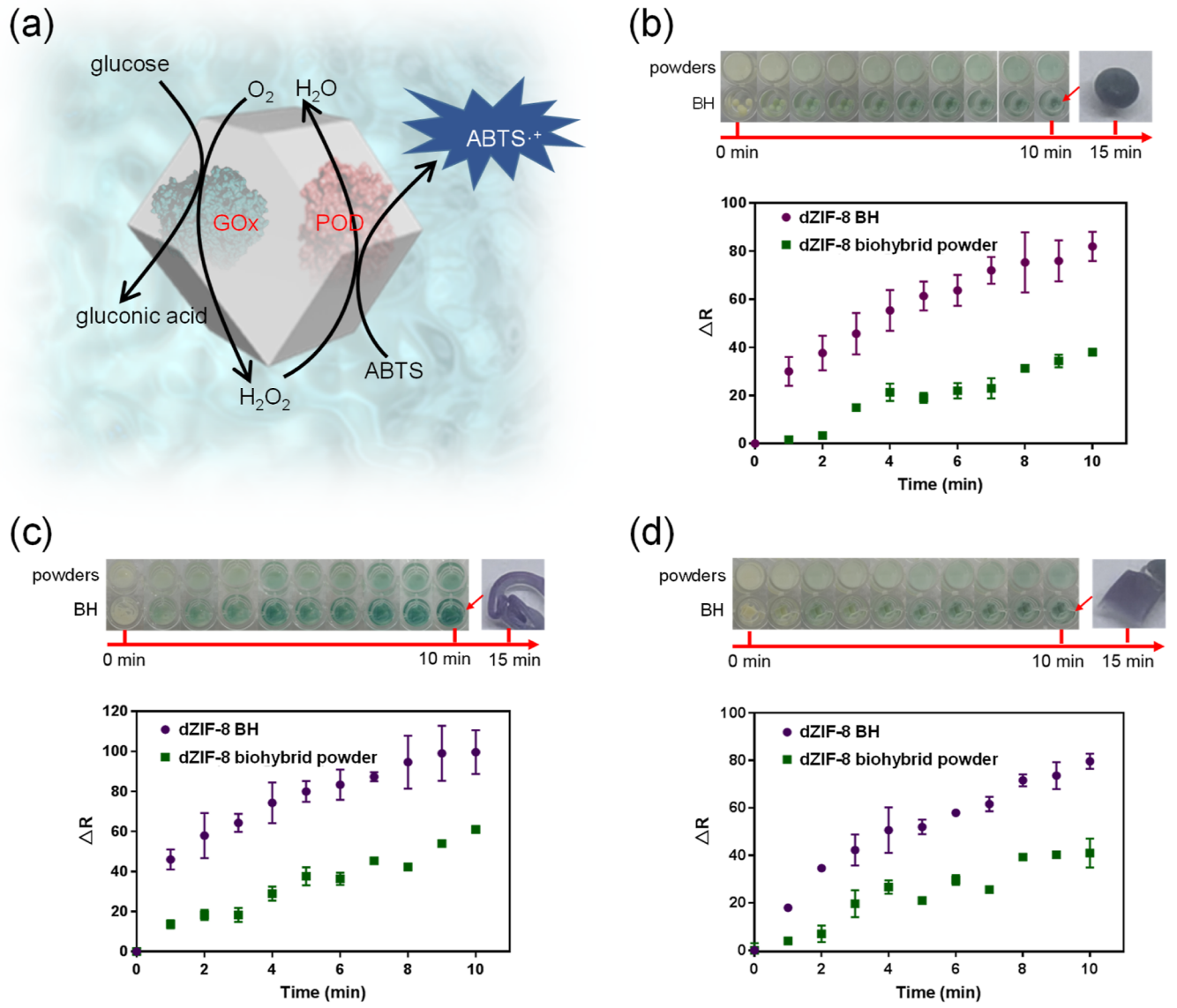

Figure 3. (a) Colorimetric sensing of glucose by the biocatalytic cascade. The real pictures of sensing glucose using dZIF-8 biohybrid powders and the prepared dZIF-8 BH: (b) bead-like dZIF-8 BH; (c) fiber-like dZIF-8 BH; and (d) sheet-like dZIF-8 BH. Glucose concentration in each assay was 1 mM.

sheet biosensor was in proportion to the glucose concentration in two sections, corresponding to the apparent color change from faint yellow to green and from green to blue-violet, respectively. Such a quantitative range of 0.05−4 mM well met the requirement for diabetes diagnosis because a patient could be diagnosed if the blood glucose level is greater than 7.0 mM.[40] In addition, owing to the high selectivity of enzymatic catalysis, the biocascade-driven sensing pathway afforded this portable biosensor with ultrahigh specificity toward glucose, as evidenced by the fact that a very limited color change was observed when adding 14 kinds of other biomolecules with a 10-fold high concentration compared to glucose (Figures 4b and S18). Furthermore, the further cross-test also verified the high selectivity of this portable biosensor (Figure S19).

Besides the sensitivity and selectivity, the mechanical strength and stability are of significant importance because both of them determine the life-time and cost of a biosensor. To demonstrate the positive effect of the double-crosslinked gelatinization on mechanical strength, the dZIF-8 BH prepared by simple crosslinking of Ca^{2+} ions and alginate was also prepared. Figure S20 describes the stress−stretch curves of the dZIF-8 BH sheet at room temperature. Compared to that of the dZIF-8 BH sheet prepared by simple Ca^{2+}−alginate crosslinking, the strength of our dZIF-8 BH sheet increased from 380 to 460 kPa, suggesting that the double-crosslinked gelatinization could improve the mechanical strength of the biosensor. Even though the stretchability of our dZIF-8 BH sheet was decreased in the stress−stretch test, it still could be folded and stretched without breakage (Figure 4c).

We next examined the stability of this biosensor in terms of the activity change after placing it at room temperature for a period. As shown in Figure 4d, our dZIF-8 BH biosensor well preserved its sensing capacity even after 30 d, and the structure of dZIF-8 was intact, as evidenced by the PXRD patterns and SEM images (Figure S21). As a comparison, the biosensor, wherein the enzymes were directly embedded into the hydrogels by a similar gelatinization (denoted as a free enzyme biosensor), dropped its sensing capacity to 48.2% after 5 d and

https://doi.org/10.1021/acs.analchem.2c03138
Anal. Chem. 2022, 94, 14385−14393

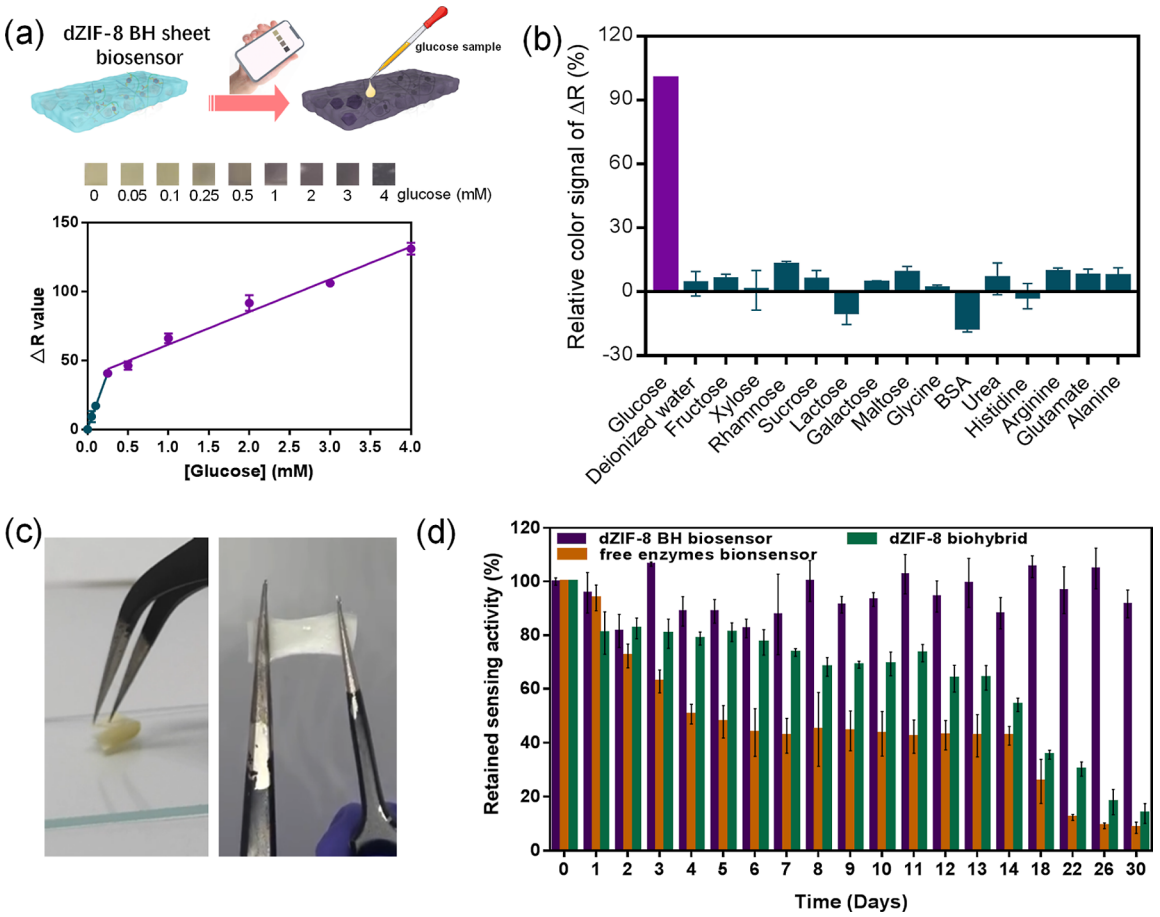

Figure 4. (a) Schematic representation of the dZIF-8 BH portable biosensor for glucose detection and the linear range for quantification. Incubation time: 15 min. (b) Selectivity of the biosensor toward glucose. Testing condition: 1 mM glucose; 10 mM interferents; incubation for 15 min. (c) Stretchability and strength of the dZIF-8 BH biosensor. (d) Retained sensing activity of the different biosensors after storage at room temperature for 30 d. Testing condition: 1 mM glucose; incubation for 15 min.

only retained 8.5% activity after 30 d. This suggested that the dZIF-8 shell could protect the encapsulated enzymes against denaturation at room temperature, and such stabilizations of the biomacromolecule by the porous organic framework in non-physiological conditions have also been discovered before.[15−21] In addition, the sensing stability of dZIF-8 BH also outperformed that of the dZIF-8 biohybrid powders, in which the dZIF-8 biohybrid powders lost 86.2% sensing activity after 30 d, while the dZIF-8 BH still retained 91.7% sensing activity after 30 d (Figure 4d). This was ascribed to the highly hydrophilic microenvironment created by the hydrogel, and previous reports have demonstrated that the hydrophilic surface favored the conformational preservation of an enzyme.[41,42] Furthermore, we also found that the dZIF-8 shell could prevent the enzymes from leaching from the biosensor, while undesirable leaching was observed in the free enzymes biosensor (Figure S22). These results together demonstrated that our dZIF-8 BH was feasible to be served as a robust and sensitive biosensor for point-of-care detection.

CONCLUSIONS

In summary, we reported a morphology-adjustable ZIF-8 biohybrid hydrogel based on a green and convenient alginate crosslinking method. This method addressed the bottleneck of the poor machinability of ZIF-8 biohybrid powders and facilitated the integration of the multiple functions of biocatalysis, the reticular framework, and the flexible hydrogel into an entity. The integrated biosensor could efficiently convert glucose into a colored product through the biocatalytic cascade of encapsulated enzymes, which enabled the colorimetric detection of glucose on a miniaturized MOF hydrogel with high sensitivity, selectivity, and stability. We anticipate that this biocompatible strategy may potentially be a versatile tool to advance the enzyme MOF bio-nanosystem for the next-generation biosensor.

ASSOCIATED CONTENT

Supporting Information

The Supporting Information is available free of charge at https://pubs.acs.org/doi/10.1021/acs.analchem.2c03138.

Reagents; routine instrument characterizations and electron microscopy methods; XRD, SEM, cryo-EM, FT-IR spectroscopy, TGA, N_2 adsorption/desorption isotherm, CLSM, and Raman spectroscopy data of the synthesized dZIF-8 materials; and the sensing performance of the established dZIF-8 BH biosensor (PDF)

AUTHOR INFORMATION

Corresponding Authors

Siming Huang − *Guangzhou Municipal and Guangdong Provincial Key Laboratory of Molecular Target & Clinical Pharmacology, the NMPA and State Key Laboratory of*

https://doi.org/10.1021/acs.analchem.2c03138
Anal. Chem. 2022, 94, 14385−14393

Respiratory Disease, School of Pharmaceutical Sciences and The Fifth Affiliated Hospital, Guangzhou Medical University, Guangzhou 511436, China; orcid.org/0000-0002-0912-1082; Email: huangsm@gzhmu.edu.cn

Guosheng Chen − *MOE Key Laboratory of Bioinorganic and Synthetic Chemistry, School of Chemistry, Sun Yat-sen University, Guangzhou 510275, China;* orcid.org/0000-0002-6540-7675; Email: chengsh39@mail.sysu.edu.cn

Authors

Ningyi Zhong − *MOE Key Laboratory of Bioinorganic and Synthetic Chemistry, School of Chemistry, Sun Yat-sen University, Guangzhou 510275, China*

Rui Gao − *MOE Key Laboratory of Bioinorganic and Synthetic Chemistry, School of Chemistry, Sun Yat-sen University, Guangzhou 510275, China*

Yujian Shen − *MOE Key Laboratory of Bioinorganic and Synthetic Chemistry, School of Chemistry, Sun Yat-sen University, Guangzhou 510275, China*

Xiaoxue Kou − *MOE Key Laboratory of Bioinorganic and Synthetic Chemistry, School of Chemistry, Sun Yat-sen University, Guangzhou 510275, China*

Jiayi Wu − *MOE Key Laboratory of Bioinorganic and Synthetic Chemistry, School of Chemistry, Sun Yat-sen University, Guangzhou 510275, China*

Gangfeng Ouyang − *MOE Key Laboratory of Bioinorganic and Synthetic Chemistry, School of Chemistry, Sun Yat-sen University, Guangzhou 510275, China;* orcid.org/0000-0002-0797-6036

Complete contact information is available at: https://pubs.acs.org/10.1021/acs.analchem.2c03138

Author Contributions

G.C. and S.H. designed and guided the project and wrote the manuscript. N.Z. and R.G. synthesized and characterized the biohybrid hydrogel and analyzed the results. Y.S., X.K., J.W., and G.O. participated in the discussions on the results. All authors have given approval to the final version of the manuscript.

Notes

The authors declare no competing financial interest.

■ ACKNOWLEDGMENTS

We acknowledge the financial support from the projects of the National Natural Science Foundation of China (22104159, 22174164, and 21904146) and the projects of Guangdong Basic and Applied Basic Research Foundation (2019A1515011722 and 2020A1515010824).

■ REFERENCES

(1) Dai, Y.; Liu, C. *Angew. Chem., Int. Ed.* **2019**, *58*, 12355−12368.
(2) Elledge, S. K.; Zhou, X.; Byrnes, J. R.; Martinko, A. J.; Lui, I.; Pance, K.; Lim, S. A.; Glasgow, J. E.; Glasgow, A. A.; Turcios, K.; Iyer, N. S.; Torres, L.; Peluso, M. J.; Henrich, T. J.; Wang, T. T.; Tato, C. M.; Leung, K. K.; Greenhouse, B. J.; Wells, A. *Nat. Biotechnol.* **2021**, *39*, 928−935.
(3) Mayer, M.; Baeumner, A. J. *Chem. Rev.* **2019**, *119*, 7996−8027.
(4) Pardee, K.; Green, A. A.; Takahashi, M. K.; Braff, D.; Lambert, G. J.; Lee, W.; Ferrante, T.; Ma, D.; Donghia, N.; Fan, M.; Daringer, N. M.; Bosch, I.; Dudley, D. M.; O'Connor, D. H.; Collins, J. J. *Cell* **2016**, *165*, 1255.
(5) Kevadiya, B. D.; Machhi, J.; Herskovitz, J.; Oleynikov, M. D.; Blomberg, W. R.; Bajwa, N.; Soni, D.; Das, S.; Hasan, M.; Patel, M.; Senan, A. M.; Gorantla, S.; McMillan, J.; Edagwa, B.; Eisenberg, R.; Gurumurthy, C. B.; Reid, S. M.; Punyadeera, C.; Chang, L. D.; Gendelman, H. E. *Nat. Mater.* **2021**, *20*, 593−605.
(6) Good, M. C.; Zalatan, J. G.; Lim, W. A. *Science* **2011**, *332*, 680−686.
(7) Vázquez-González, M.; Wang, C.; WillnerA, I. *Nat. Catal.* **2020**, *3*, 256−273.
(8) Yeger-Lotem, E.; Sattath, S.; Kashtan, N.; Itzkovitz, S.; Milo, R.; Pinter, R. Y.; Alon, U.; Margalit, H. *Proc. Natl. Acad. Sci. U.S.A.* **2004**, *101*, 5934−5939.
(9) Wilner, O. I.; Weizmann, Y.; Gill, R.; Lioubashevski, O.; Freeman, R.; Willner, I. *Nat. Nanotechnol.* **2009**, *4*, 249−254.
(10) Fu, J.; Liu, M.; Liu, Y.; Woodbury, N. W.; Yan, H. *J. Am. Chem. Soc.* **2012**, *134*, 5516−5519.
(11) Sheldon, R. A.; Basso, A.; Brady, D. *Chem. Soc. Rev.* **2021**, *50*, 5850−5862.
(12) Liese, A.; Hilterhaus, L. *Chem. Soc. Rev.* **2013**, *42*, 6236−6249.
(13) Lian, X.; Fang, Y.; Joseph, E.; Wang, Q.; Li, J.; Banerjee, S.; Lollar, C.; Wang, X.; Zhou, H.-C. *Chem. Soc. Rev.* **2017**, *46*, 3386−3401.
(14) Li, P.; Chen, Q.; Wang, T. C.; Vermeulen, N. A.; Mehdi, B.; Dohnalkova, A.; Browning, N. D.; Shen, D.; Anderson, R.; Gómez-Gualdrón, D. A.; Cetin, F. M.; Jagiello, J.; Asiri, A. M.; Stoddart, J.; Farha, O. K. *Chem* **2018**, *4*, 1022−1034.
(15) Liang, W.; Wied, P.; Carraro, F.; Sumby, C. J.; Nidetzky, B.; Tsung, C.-K.; Falcaro, P.; Doonan, C. J. *Chem. Rev.* **2021**, *121*, 1077−1129.
(16) Lyu, F.; Zhang, Y.; Zare, R. N.; Ge, J.; Liu, Z. *Nano Lett.* **2014**, *14*, 5761−5765.
(17) Liang, W.; Xu, H.; Carraro, F.; Maddigan, N. K.; Li, Q.; Bell, S. G.; Huang, D. M.; Tarzia, A.; Solomon, M. B.; Amenitsch, H.; Vaccari, L.; Sumby, C. J.; Falcaro, P.; Doonan, C. J. *J. Am. Chem. Soc.* **2019**, *141*, 2348−2355.
(18) Chen, G.; Huang, S.; Kou, X.; Wei, S.; Huang, S.; Jiang, S.; Shen, J.; Zhu, F.; Ouyang, G. *Angew. Chem., Int. Ed.* **2019**, *58*, 1463−1467.
(19) Liao, F. S.; Lo, W. S.; Hsu, Y. S.; Wu, C. C.; Wang, S. C.; Shieh, F. K.; Morabito, J. V.; Chou, L. Y.; Wu, K. C. W.; Tsung, C. K. *J. Am. Chem. Soc.* **2017**, *139*, 6530−6533.
(20) Chen, G.; Huang, S.; Kou, X.; Zhu, F.; Ouyang, G. *Angew. Chem., Int. Ed.* **2020**, *59*, 13947−13954.
(21) Liang, K.; Ricco, R.; Doherty, C. M.; Styles, M. J.; Bell, S.; Kirby, N.; Mudie, S.; Haylock, D.; Hill, A. J.; Doonan, C. J.; Falcaro, P. *Nat. Commun.* **2015**, *6*, 7240.
(22) Chen, W.-H.; Vázquez-González, M.; Zoabi, A.; Abu-Reziq, R.; Willner, I. *Nat. Catal.* **2018**, *1*, 689−695.
(23) Wu, X.; Yue, H.; Zhang, Y.; Gao, X.; Li, X.; Wang, L.; Cao, Y.; Hou, M.; An, H.; Zhang, L.; Li, S.; Ma, Y.; Lin, H.; Fu, W.; Gu, W.; Lou, R. N.; Wei, J.; Zare, R. N.; Ge, J. *Nat. Commun.* **2019**, *10*, 5165.
(24) Chen, G.; Kou, X.; Huang, S.; Tong, L.; Shen, Y.; Zhu, W.; Zhu, F.; Ouyang, G. *Angew. Chem., Int. Ed.* **2020**, *59*, 2867−2874.
(25) Hu, C.; Bai, Y.; Hou, M.; Wang, Y.; Wang, L.; Cao, X.; Chan, C.; Sun, H.; Li, W.; Ge, J.; Ren, K. *Sci. Adv.* **2020**, *6*, No. eaax5785.
(26) Tong, L.; Huang, S.; Shen, Y.; Liu, S.; Ma, X.; Zhu, F.; Chen, G.; Ouyang, G. *Nat. Commun.* **2022**, *13*, 951.
(27) Liang, J.; Liu, J. M. S.; Lord, Y.; Wang, K.; Liang, K. *Small* **2021**, *17*, 2103590.
(28) Liu, J.; Xue, J.; Fu, L.; Xu, J.; Lord, M. S. K.; Liang, K. *Adv. Funct. Mater.* **2022**, *32*, 2111271.
(29) Guo, Z.; Wu, Y.; Xie, Z.; Shao, J.; Liu, J.; Yao, Y.; WangShen, J. Y.; Gooding, J. J.; Liang, K. *Angew. Chem., Int. Ed.* **2022**, *61*, No. e202209747.
(30) Hecht, H.; Srebnik, S. *Biomacromolecules* **2016**, *17*, 2160−2167.
(31) Wang, N.; Yang, L.-Y.; Wang, Y.-g.; Ouyang, X.-k. *Polymers* **2018**, *10*, 750.
(32) Yang, S.; Peng, L.; Syzgantseva, O. A.; Trukhina, O.; Kochetygov, I.; Justin, A.; Sun, D. T.; Abedini, H. M.; Syzgantseva, A.; Oveisi, E.; Lu, G.; Queen, W. L. *J. Am. Chem. Soc.* **2020**, *142*, 13415−13425.

(33) Chen, G.; Huang, S.; Shen, Y.; Kou, X.; Ma, X.; Huang, S.; Tong, Q.; Ma, K.; Chen, W.; Wang, P.; Shen, J.; Zhu, F.; Ouyang, G. *Chem* **2021**, *7*, 2722−2742.
(34) Chen, G.; Tong, L.; Huang, S. S. F.; Huang, G.; Zhu, F.; Ouyang, G. *Nat. Commun.* **2022**, *13*, 4816.
(35) Bradford, M. M. *Anal. Biochem.* **1976**, *72*, 248−254.
(36) Park, K. S.; Ni, Z.; Côté, A. P.; Choi, J. Y.; Huang, R. D.; Uribe-Romo, F. J.; Chae, H. K.; O'Keeffe, M.; Yaghi, O. M. *Proc. Natl. Acad. Sci. U.S.A.* **2006**, *103*, 10186−10191.
(37) Shen, B.; Chen, X.; Shen, K.; Xiong, H.; Wei, F. *Nat. Commun.* **2020**, *11*, 2692.
(38) de Graaf, S.; Momand, J.; Mitterbauer, C.; Lazar, S.; Kooi, B. J. *Sci. Adv.* **2020**, *6*, No. eaay4312.
(39) El Boukari, M.; Bribes, J. L.; Maillols, J. *J. Raman Spectrosc.* **1990**, *21*, 755−759.
(40) Yetisen, A. K.; Jiang, N.; Fallahi, A.; Montelongo, Y.; Ruiz-Esparza, G. U.; Tamayol, A.; Zhang, Y. S.; Mahmood, I.; Yang, S.-A.; Kim, K. S.; Butt, H.; Khademhosseini, A.; Yun, S. H. *Adv. Mater.* **2017**, *29*, 1606380.
(41) Melik-Nubarov, N. S.; Mozhaev, V. V.; Šikšnis, S.; Martinek, K. *Biotechnol. Lett.* **1987**, *9*, 725−730.
(42) Mozhaev, V. V.; Aiksnis, V. A.; Melik-Nubarov, N. S.; Galkantaite, N. Z.; Denis, G. J.; Butkus, E. P.; Zaslavsky, B. Y.; Mestechkina, N. M.; Martinek, K. *Eur. J. Biochem.* **1998**, *173*, 147−154.

https://doi.org/10.1021/acs.analchem.2c03138
Anal. Chem. 2022, 94, 14385−14393